Modeling the Pulse Profiles of Millisecond Pulsars in the Second LAT Catalog of Gamma-ray Pulsars

T. J. Johnson[1], A. K. Harding[2], C. Venter[3], & J. E. Grove[4]
on behalf of the *Fermi* LAT Collaboration and Pulsar Timing Consortium

We outline techniques for simulating and fitting MSP pulse profiles and present preliminary results using light curves from the second LAT pulsar catalog.

Abstract:

Significant gamma-ray pulsations have been detected from ~40 millisecond pulsars (MSPs) using 3 years of sky-survey data from the *Fermi* LAT and radio timing solutions from across the globe [5]. We have fit the radio and gamma-ray pulse profiles of these MSPs using geometric versions of slot gap, outer gap, and pair-starved polar cap gamma-ray emission models and radio cone and core models. For MSPs with radio and gamma-ray peaks aligned in phase we also explore low-altitude slot gap gamma-ray models and caustic radio models. The best-fit parameters provide constraints on the viewing geometries and emission sites. While the exact pulsar magnetospheric geometry is unknown, we can use the increased number of detected gamma-ray MSPs to look for significant trends in the population which average over these uncertainties.

Light Curve Simulation and Fitting:

Using the vacuum retarded-dipole magnetic field geometry [6], we have simulated MSP light curves using geometric outer gap (OG) [7], slot gap/two-pole caustic (TPC) [8], pair-starved polar cap (PSPC) [9], and low-altitude slot gap (laSG) [10] gamma-ray models with either a single-altitude hollow-cone and/or core beam [11], altitude-limited TPC/OG [10], or laSG radio models. Uniform emissivity, in the co-rotating frame, is assumed along the field lines except in the laSG and PSPC simulations.

Gamma-ray profiles are fit using Poisson likelihood and radio profiles are fit using a χ^2 statistic. We scan over the model phase space and estimate uncertainties on the best-fit parameters from either 1- or 2-D likelihood profiles.

Following [10] we sort the observed MSP light curves into 3 model classes.

Class I (26 MSPs): the gamma-ray peaks lag the main radio component.

Class II (6 MSPs): the gamma-ray and radio components are aligned in phase.

Class III (6 MSPs): the gamma-ray peaks lead the main radio component.

Emission Geometries:

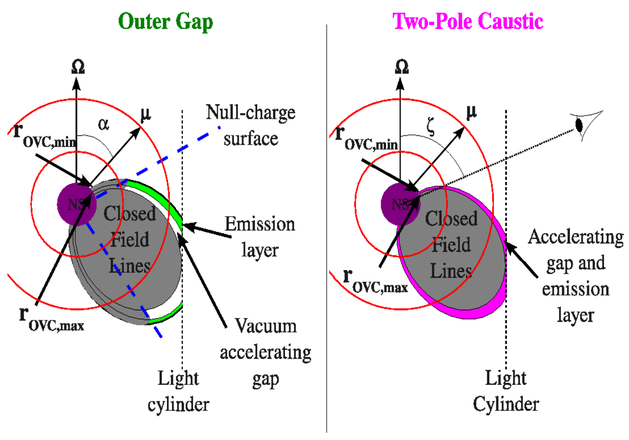

Reproduced from [10], toroidal field components suppressed and emission zones symmetric about μ not shown. No emission comes from gray regions. The red circles are example minimum and maximum (R_{max}) emission altitudes. For all models $R_{max} \leq 1.2$ light cylinder radii but no emission is collected outside the light cylinder.

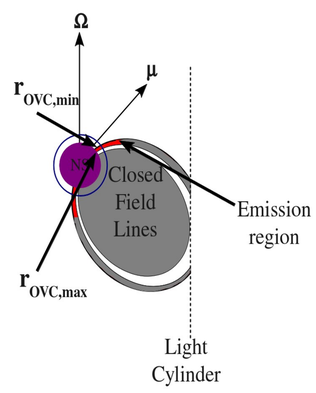

Emission geometry for the laSG model. Blue circle represents where the emission peaks and falls off as an asymmetric Gaussian above and below. This geometry is assumed for both the radio and gamma-ray beams, possibly with different gap parameters.

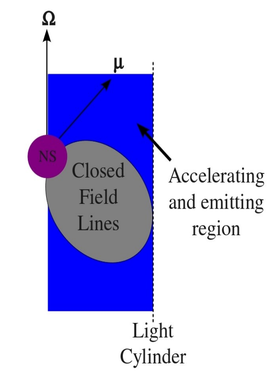

Emission geometry for the PSPC model. Only part of the emitting and accelerating region is shown.

Polarization information helps discriminate between different radio models. The hollow-cone predicts some degree of linear polarization, sense-changing circular polarization suggests the presence of a core beam, and a lack of polarization may be indicative of caustic radio emission (alTPC/OG) [10].

Population Properties:

The magnetic field geometry we've used is only an approximation; however, fitting many MSPs allows us to marginalize over uncertainties introduced by using an incorrect field geometry and look for meaningful trends in the population as a whole.

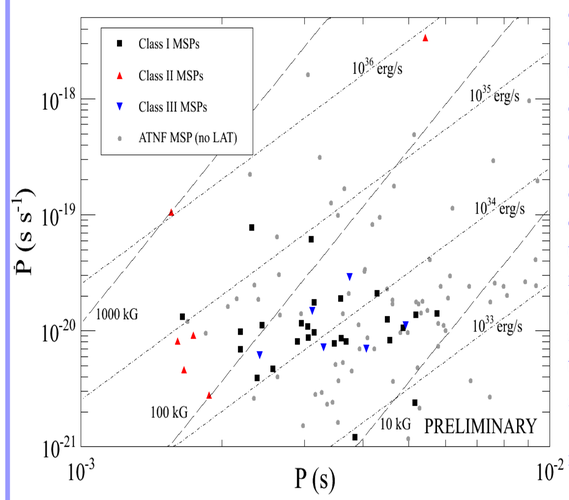

$\dot{P}$ vs P with lines of constant magnetic field at the light cylinder (B_{LC}, dashed) and rotational energy loss rate ($\dot{E}$, dot-dashed) for 38 LAT-detected MSPs, sorted by class, and other MSPs in the ATNF database. $\dot{P}$ is corrected for the Shlovskii effect where applicable. Class II MSPs tend to have higher B_{LC} and $\dot{E}$ (as noted by [12,13]) but clearly that isn't the whole story.

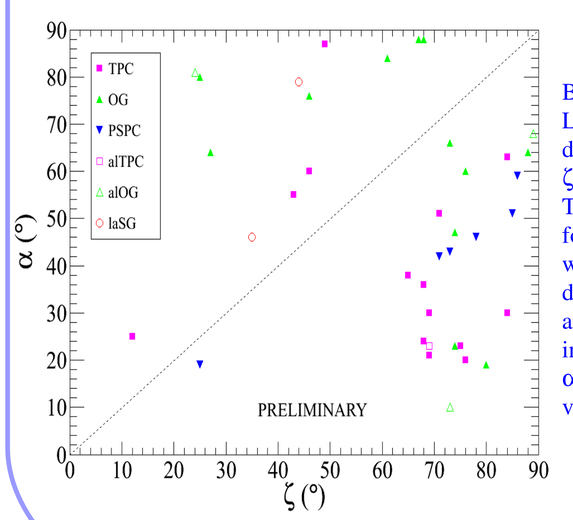

Best-fit (ζ,α) pairs for 38 LAT-detected MSPs, the dashed line indicates α = ζ (the magnetic axis). There is a clear preference for large ζ (consistent with a random, angular distribution of spin axes and also necessary to intersect caustics for low α). The distribution of α values is nearly uniform.

Class I

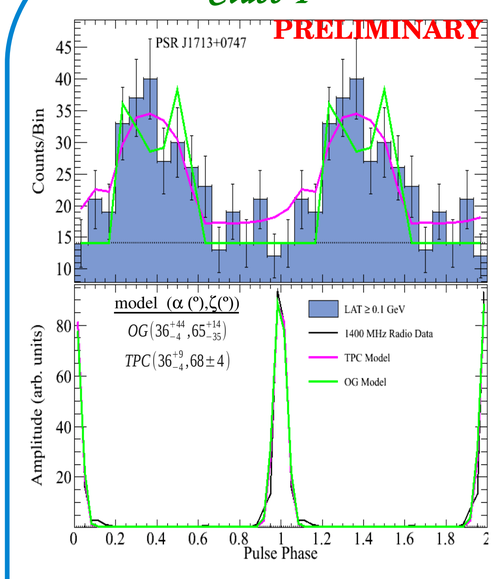

Fits for PSR J1713+0747 using TPC and OG models. Polarimetry suggests the presence of a core beam, neglecting this in the model can lead to differences in α and ζ of as much as 30°.

Class II

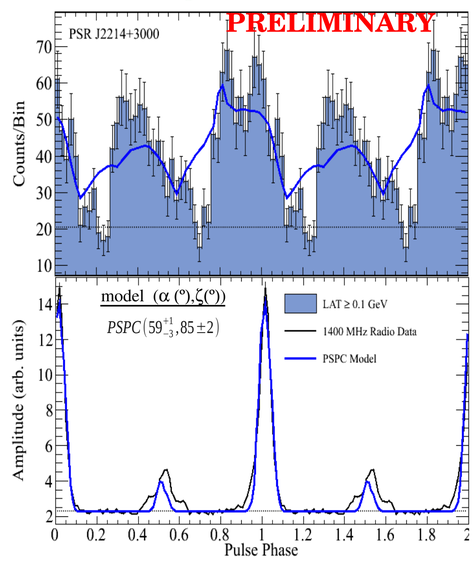

Fits for PSR J2214+3000 using the PSPC model.

Class III

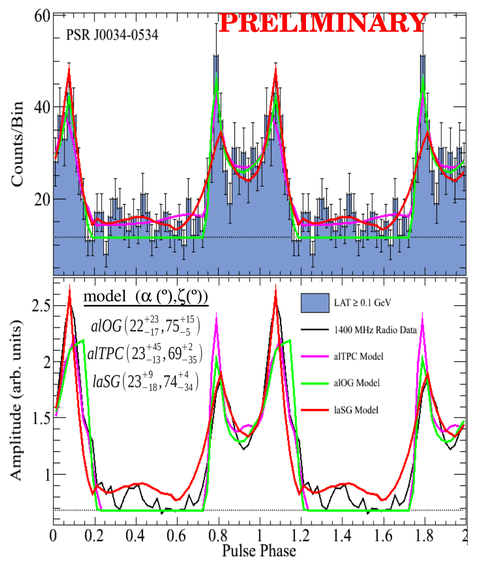

Fits for PSR J0034-0534 using the alTPC/OG and laSG models. Measured 0% polarization is consistent with caustic radio emission.

Estimated uncertainties are 95% confidence level from 2-D likelihood profiles.

Future:

We have fit the unweighted-counts profiles of almost all MSPs in the second pulsar catalog and have begun to look for population trends in viewing geometry, energetics, and best-fit model with a larger sample than [12]. The best-fit geometries suggest a uniform distribution in α which is contrary to some expectations [14,15] and may suggest movement towards an orthogonal configuration as MSPs (which have lower magnetic fields than non-recycled pulsars) spin down.

Now that we have a large sample of fits using these simulations, we can investigate how the best-fit values scale with population variables, test different magnetic field geometries, explore radio cone/core models at different altitudes from [11], and investigate mixtures of caustic and non-caustic radio emission.

***Affiliations*:**

1. National Research Council Fellow resident at the Naval Research Laboratory
2. NASA Goddard Space Flight Center
3. North-West University, South Africa
4. Naval Research Laboratory

***References*:**

5. Abdo et al. *in preparation*
6. Deutsch, Anns. d'Astrophys., **18**, 1 (1955)
7. Romani & Yadigaroglu, ApJ, **438**, 314 (1995)
8. Dyks & Rudak, ApJ, **598**, 1201 (2003)
9. Harding et al., ApJ, **622**, 531 (2005)
10. Venter, Johnson, & Harding, ApJ, **744**, 34 (2012)
11. Story et al., ApJ, **671**, 713 (2007)
12. Johnson, PhD Thesis, Univeristy of Maryland (2011) (arXiv:1209.4000)
13. Espinoza et al. *submitted*
14. Young et al., MNRAS, **402**, 1317 (2010)
15. Ruderman, ApJ, **366**, 261 (1991)

***Acknowledgments*:**

The *Fermi* LAT Collaboration acknowledges support from a number of agencies and institutes for both development and the operation of the LAT as well as scientific data analysis. These include NASA and DOE in the United States, CEA/Irfu and IN2P3/CNRS in France, ASI and INFN in Italy, MEXT, KEK, and JAXA in Japan, and the K. A. Wallenberg Foundation, the Swedish Research Council and the National Space Board in Sweden. Additional support from INAF in Italy and CNES in France for science analysis during the operations phase is also gratefully acknowledged. Part of this work is performed at NRL sponsored by NASA DPR S-15633-Y.